



# A sensitive acetaminophen sensor based on Co metal–organic framework (ZIF-67) and macroporous carbon composite

Jing Tang\*<sup>ORCID</sup>, Zhen-Zhen Hui, Tao Hu, Xin Cheng, Jia-Hao Guo, Zi-Rong Li, Hao Yu\*<sup>ORCID</sup>

Received: 23 June 2020/Revised: 10 September 2020/Accepted: 16 January 2021/Published online: 15 May 2021  
© Youke Publishing Co., Ltd. 2021

**Abstract** The composite of zeolitic imidazolate frameworks (ZIF-67) and ordered macroporous carbon (OMC) was successfully synthesized via in situ growth from the OMC matrix. The ZIF67–OMC composite was verified by scanning electron microscopy (SEM) and transmission electron microscopy (TEM), powder X-ray diffraction (XRD) and electrochemical impedance spectroscopy (EIS) and then evaluated as a modified material for electrochemical sensor. Benefitting from the large surface area and enhanced conductivity of the ZIF67–OMC composite, ZIF67–OMC nanocomposite showed superior electrocatalytic performance toward acetaminophen (AP) oxidation. The redox reaction of AP underwent a quasi-reversible redox reaction with higher anodic current at ZIF67–OMC modified electrode compared with the bare glassy carbon electrode (GCE). In optimal condition, the ZIF67–OMC/GCE was stable, reproducible and had a linear range of 0.05–100  $\mu\text{mol}\cdot\text{L}^{-1}$  AP concentration, with the detection limit of 20  $\text{nmol}\cdot\text{L}^{-1}$  (signal-to-noise of  $S/N = 3$ ). In addition, the prepared sensing platform for the detection of AP was evaluated for the compound paracetamol tablets and urine samples.

**Keywords** Macroporous carbon; ZIF-67; Acetaminophen; Modified electrode

## 1 Introduction

As a common antipyretic and analgesic medicine, acetaminophen (AP) is widely used to relieve the moderate pains and reduce the fevers with the advantages of low irritation and less allergic reactions [1, 2]. However, the excessive dosage of AP is responsible for accumulation of toxic metabolites in liver and kidney, subsequently causing fatal hepatotoxicity and nephrotoxicity [3]. Thus, monitoring the AP is essential for public health care and drug safety. It is desirable to develop a fast and sensitive method to determine AP to ensure the human health for the drug industry.

To date, many analytical methods, such as spectrophotometry [4], chromatography [5, 6] and chemiluminescence [7], have been established for the detection of AP. However, most of the above methods have intrinsic shortcomings such as complicated preprocessing and high cost. Electrochemical technique is more advantageous than other techniques because of its low cost, high sensitivity and speed [8]. Although some electrochemical sensors for detecting AP have been developed [9], their low current signal and linear range are still major obstacles for detecting AP. Some attempts have been carried out by various material-modified electrodes, for instance, graphene [10–12], metal nanoparticles, metal oxide [13, 14], carbon nanotubes [15] and conductive polymers [16]. Hence, it is still essential to develop a novel electrochemical approach for the detection of AP with better performance.

Nowadays, more and more researchers begin to focus on a class of porous materials, metal–organic frameworks (MOFs), which are composed of metal cluster and organic linkers by coordinative bonding. MOFs can be applied in many fields including gas absorption and separation [17], electronic and optoelectronic [18–20], energy storage and catalysis [21–24]

J. Tang\*, Z.-Z. Hui, T. Hu, X. Cheng, J.-H. Guo, Z.-R. Li, H. Yu\*  
College of Chemistry and Material Engineering, Anhui Science and Technology University, Bengbu 233030, China  
e-mail: zhengtang102@163.com

H. Yu  
e-mail: yhz\_1230@163.com



because they have the intrinsic virtues of high specific surface area, large pore volume and low density [25]. However, most MOFs have the disadvantages of poor stability and low conductivity [26]. The couple of semiconductive material and conductive material is developed to solve this problem. Normally, MOF-based electrodes are integrated with materials which have high electrochemical activity, such as metal nanoparticles [27, 28], organic molecules [29] and conductive carbon materials [30, 31]. In particular, the performance of carbon materials in improving the electrode conductivity is preferable. For example, the combination of polyoxometalate nanoparticles and zeolitic imidazolate frameworks (ZIF-8@ZIF-67) via the coprecipitation process improved the electrochemical performance of oxygen evolution reaction [28]. Wang and coworkers [30] reported nickel-based metal-organic frameworks (DUT-9)/mesoporous carbon composites by in situ growth for the detection of baicalein. As one member of carbon materials, ordered macroporous carbon (OMC) has been considered to be a promising candidate for sensing materials due to its large surface area, superior conductivity and good mechanical stability [32–35]. In particular, OMC can be used as a platform for supporting MOFs to form a new composite material [36]. Zeolitic imidazolate frameworks-67 (ZIF-67) are a representative member of Co-based MOFs [37], which has tunable pore sizes and catalytic properties in structure as well as high chemical and thermal stabilities in function [38]. Moreover, the development of multifunctional applications of ZIF-67 has received increasing scientific interest because different functional groups could be incorporated into the ZIF-67 and it exhibits excellent prospects for electrochemical research.

Taking into account the characteristics of ZIF-67 and OMC, as illustrated in Scheme 1, the special structure of electrocatalytic materials based on ZIF67-OMC nanocomposite was successfully fabricated via in situ growth method. Interestingly, the size of ZIF-67 was matched with the macropores of the OMC matrix. ZIF67-OMC composite was electrodeposited on the bare GCE and used as a novel acetaminophen sensor. As far as we know, there is no report of AP detection based on the modification of GCE with ZIF67-OMC composite. The ZIF67-OMC modified electrode utilized the high surface area and the porosity structure of ZIF-67 crystal as well as the electron conductivity of OMC, which exhibited excellent electrocatalytic performance of AP.

## 2 Experimental

### 2.1 Materials

Co(NO<sub>3</sub>)<sub>2</sub>·6H<sub>2</sub>O, acetaminophen (AP), 2-methylimidazole (2-melm), dopamine (DA), ascorbic acid (AA), glucose,

citric acid, tyrosine and other chemicals were obtained from Aladdin Industrial Co. Ltd. (China). A series of Britton–Robinson (B–R) buffer with different pH was made from 0.04 mol·L<sup>-1</sup> H<sub>3</sub>BO<sub>3</sub>, H<sub>3</sub>PO<sub>4</sub> and CH<sub>3</sub>COOH, and then adjusting the pH with 0.20 mol·L<sup>-1</sup> NaOH. All other reagents were of at least analytical purity and used as without further processing.

### 2.2 Apparatus

The phase structure of prepared material was verified by X-ray diffraction (XRD) on a Bruker diffractometer (D8-Advance, Germany). The morphology of the sample was taken on a Carl Zeiss EVO18 scanning electron microscope (SEM, Germany) at 5 kV and a JEOL JEM-2010 transmission electron microscope (TEM, Japan) at 30 kV. All electrochemical experiments were performed on a CHI 660E electrochemical workstation (Chenhua, China) with a standard electrode cell, which contained the bare GCE, OMC, ZIF-67 or ZIF67-OMC modified electrode (diameter of 3 mm) as working electrode, a saturated calomel electrode (SCE) and a Pt wire as the reference and auxiliary electrodes, respectively.

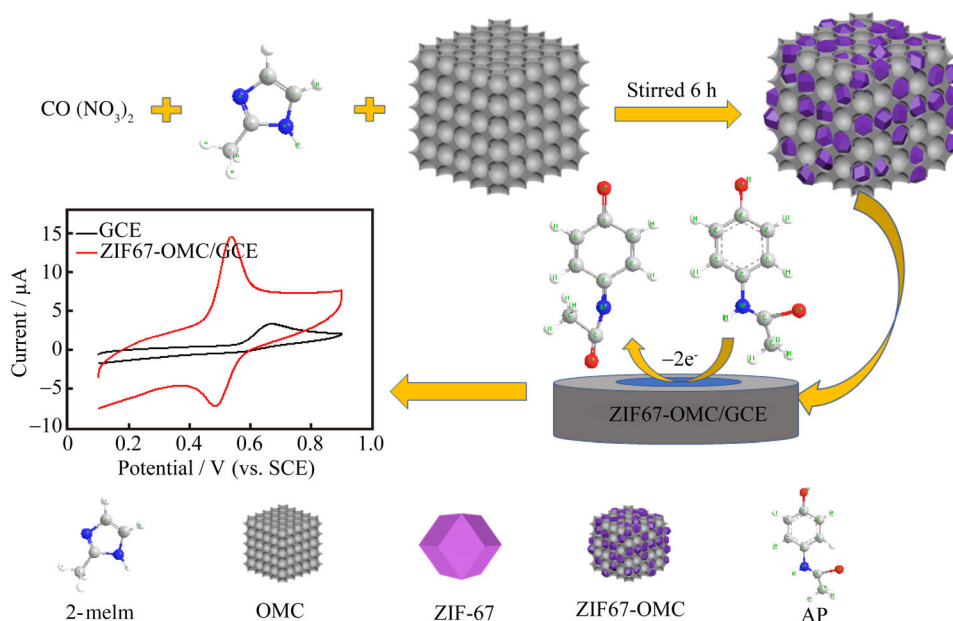
### 2.3 Synthesis of ZIF67-OMC

OMC was prepared based on the previous report [39]; 2 g SiO<sub>2</sub> and 2 g sucrose (containing 0.15 ml of H<sub>2</sub>SO<sub>4</sub>) were added in deionized water and maintained at 100 °C for 6 h and at 160 °C for another 6 h to ensure carbonized sucrose inside the gaps of the SiO<sub>2</sub> particles. The carbonization was subsequently carried out at 900 °C for 3 h in N<sub>2</sub> atmosphere. At last, the SiO<sub>2</sub> template was etched away by placing the calcined product in 20% aqueous HF. The synthesis of ZIF-67 was described in our previous literature [40].

The acid-pretreated OMC (35 mg) and PVP (175 mg) were dissolved in methanol (25 ml) ultrasonically. Next, 500 mg of Co(NO<sub>3</sub>)<sub>2</sub>·6H<sub>2</sub>O and 750 mg of 2-melm were dispersed in the above solution under stirring for 2 h and then incubated for 24 h at 25 °C. Subsequently, the solid was centrifuged and washed with methanol three times. Finally, the products were vacuum dried at 60 °C for 12 h to get ZIF67-OMC composite.

### 2.4 Electrochemical experiments

Prior to modification, the bare GCE (with diameter of  $d = 3.0$  mm) was polished with 0.3 and 0.05 μm alumina powder on a felt pad and treated ultrasonically in ethanol and deionized water to remove away the impurities. ZIF67-OMC composite (2 mg) was dispersed with DMF (2 ml, containing 0.1 mol·L<sup>-1</sup> NaNO<sub>3</sub>) and sonicated for



**Scheme 1** Fabrication process of ZIF67–OMC modified electrode and electrochemical determination of acetaminophen (AP)

10 min to obtain the homogeneous brown suspension. The deposition of ZIF67–OMC was carried out in the above suspension via cyclic voltammetry between  $-1.0$  and  $1.5$  V for 15 cycles at  $100 \text{ mV}\cdot\text{s}^{-1}$ . Then, ZIF67–OMC modified electrode was obtained. ZIF-67/GCE and OMC/GCE were also prepared for comparison.

### 3 Results and discussion

#### 3.1 Characterization of ZIF67–OMC composite

Figure 1 gives the XRD patterns of the ZIF-67 and composite of ZIF67–OMC. As shown, the diffraction peaks of as-prepared ZIF-67 were found to be in accordance with those of the simulated ZIF-67 crystal, demonstrating the successful synthesis of ZIF-67 crystal. The characteristic XRD pattern of ZIF67–OMC was basically consistent with that of pure ZIF-67 crystal, suggesting that the phase purity and crystallinity of ZIF-67 in the composite were almost unchanged after the introduction of OMC. Besides, a weak broad diffraction peak at  $24^\circ$  was assigned to the typical (002) plane of the OMC [41]. Hence, the above results indicated the successful fabrication of ZIF67–OMC.

SEM and TEM images of the prepared OMC and ZIF67–OMC are depicted in Fig. 2. There were lots of uniform macropores with the pore size of  $\sim 450$  nm in the OMC (Fig. 2a), which was matched with the TEM image (Fig. 2c). In the presence of OMC, ZIF-67 grew within the pores of the OMC matrix. As shown in Fig. 2b, d, the ZIF-67 crystal with a

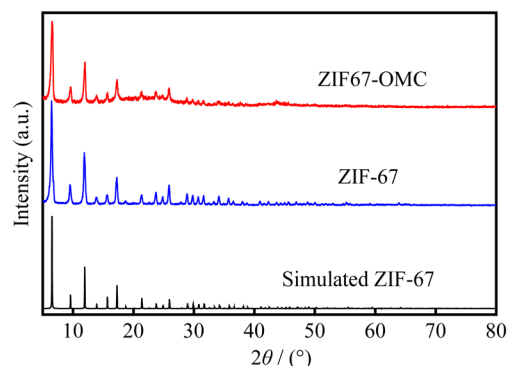


**Fig. 1** XRD patterns of ZIF-67 and ZIF67–OMC composite

well dodecahedron shape was embedded in OMC of the composite. The average size of ZIF-67 crystal was  $\sim 400$  nm. These phenomena further confirmed that the ZIF67–OMC sample was comprised of OMC and ZIF-67. Energy-dispersive spectroscopy (EDS) mappings (Fig. 2e–i) were conducted to illustrate the component analysis of ZIF67–OMC, suggesting that C, Co, N and O elements were distributed on the surface of ZIF67–OMC uniformly. The result further verified the formation of the ZIF67–OMC.

#### 3.2 Electrochemical characterization of ZIF67–OMC modified electrode

The electrochemical activities of different electrodes were investigated by cyclic voltammetry (CV) as the probe of  $[\text{Fe}(\text{CN})_6]^{3-/4-}$  ( $5.0 \text{ mmol}\cdot\text{L}^{-1}$ ). In Fig. 3a, a pair of redox peaks is observed with the difference between the anodic and cathodic peak potential ( $\Delta E_p$ ) of  $85 \text{ mV}$  at the bare

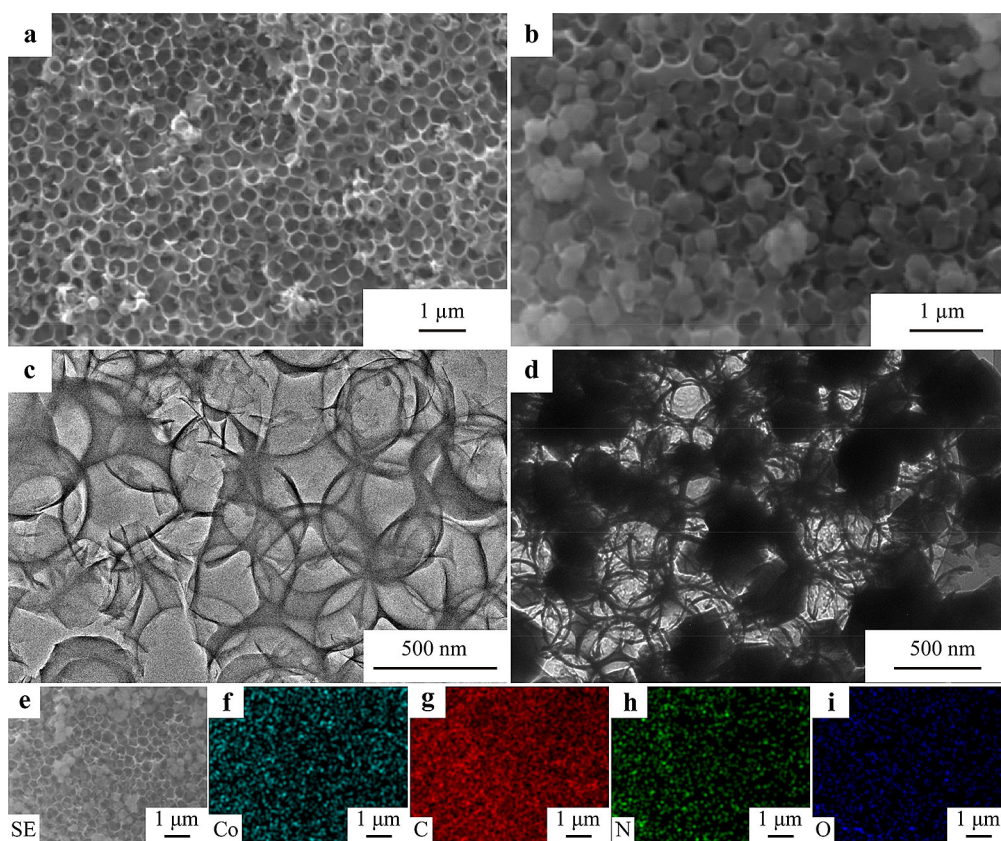


**Fig. 2** SEM images of **a** OMC and **b** ZIF67-OMC composite; TEM images of **c** OMC and **d** ZIF67-OMC composite; **e-i** EDS mapping images of Co, C, N and O

GCE. For ZIF-67/GCE,  $\Delta E_p$  of the anode and cathode peak increased to 240 mV with low peak currents owing to the low conductivity of ZIF-67. When OMC was dropped into the bare GCE, the currents of the redox peaks apparently increased and  $\Delta E_p$  decreased to 80 mV, suggesting that OMC had high conductivity to improve the electron transfer. After the GCE surface was electrodeposited with

the ZIF67-OMC composite, the  $\Delta E_p$  decreased from 80 to 74 mV with the highest current signal. The above behaviors demonstrated that the ZIF67-OMC composite facilitated fast electron transfer between electrode surface and the analyte.

The electrode effective area was obtained by Randles-Sevcik equation. The anodic peak currents ( $I_p$ ) of the probe

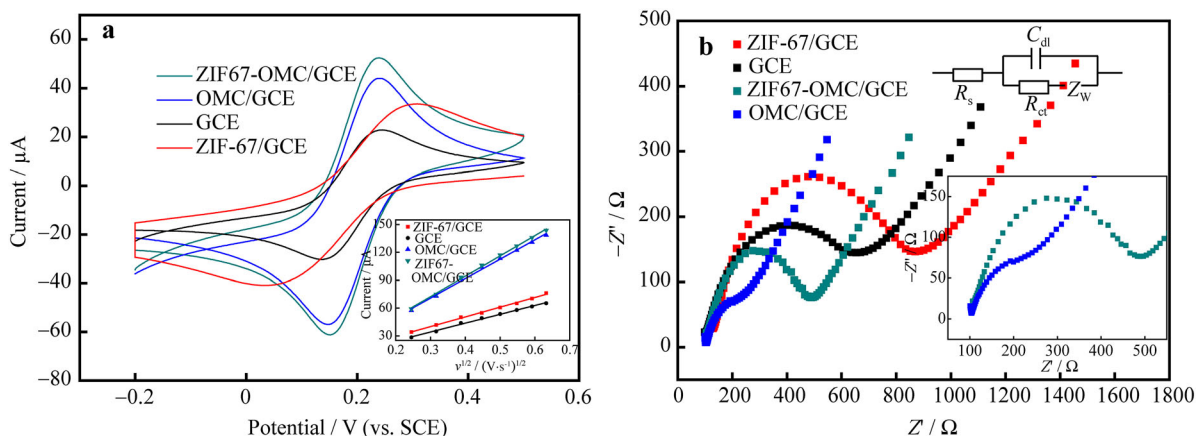


**Fig. 3** **a** CVs and **b** Nyquist plots of bare GCE, ZIF-67/GCE, OMC/GCE and ZIF67-OMC/GCE in 5.0 mmol·L<sup>-1</sup> [Fe(CN)<sub>6</sub>]<sup>3-/4-</sup> containing 0.1 mol·L<sup>-1</sup> KCl (inset in **a**: plot of  $I_p$  vs.  $v^{1/2}$  curves; inset in **b**: Randles equivalent electrical circuit and enlargement of plots of OMC/GCE and ZIF67-OMC/GCE, where  $Z'$  is real part of impedance,  $Z''$  is imaginary part of impedance)

increased linearly with the square root of scan rates (inset of Fig. 3a), according to Eq. (1):

$$I_p = 2.69 \times 10^5 n^{3/2} A D_0^{1/2} C_0 \nu^{1/2} \quad (1)$$

where  $A$  refers to the electrode effective area,  $n$  refers to the number of electrons transfer ( $n = 1$ ),  $C_0$  is the substrate concentration,  $\nu$  is the scan rate and  $D_0$  is the diffusion coefficient ( $7.6 \times 10^{-6} \text{ cm}^2 \cdot \text{s}^{-1}$ ). The plots of  $I_p \cdot \nu^{1/2}$  are shown in the inset of Fig. 3a, and the values of  $A$  were calculated to be 0.026, 0.028, 0.056 and 0.060  $\text{cm}^2$  for bare GCE, ZIF-67/GCE, OMC/GCE and ZIF67–OMC/GCE, respectively, demonstrating that the ZIF67–OMC composite can steadily enlarge the surface area of the electrode.

In addition, electrochemical impedance spectroscopy (EIS) technique was applied to determine the interfacial electron transfer properties of the four different electrodes. The semicircle diameter in high-frequency region of the Nyquist plots normally represents the interfacial charge transfer resistance ( $R_{ct}$ ). As depicted in Fig. 3b, the bare GCE displayed well defined semicircle with  $R_{ct}$  value of 500  $\Omega$ . At ZIF-67/GCE and the value of resistance was larger than that of the bare GCE, indicating the low electron conductivity of ZIF-67. However, the diameter of OMC/GCE decreased to  $\sim 150 \Omega$ , implying that the OMC film improved electron transfer. The  $R_{ct}$  of ZIF67–OMC/GCE (400  $\Omega$ ) was displayed because OMC was incorporated in ZIF-67 crystal, indicating that OMC played a key role in accelerating the electrons transfer.

### 3.3 Electrocatalytic performance of ZIF67–OMC/GCE toward AP

The electrocatalytic performance of AP at different electrodes was conducted by CV. Figure 4 depicts the CVs acquired for AP ( $0.10 \text{ mmol} \cdot \text{L}^{-1}$ ) in B–R buffer (pH 4.0). The electrochemical reaction of AP at the bare GC electrode was irreversible, and the only anodic peak was found at 0.670 V with the current of 2.1  $\mu\text{A}$ . With the introduction of OMC, one pair of redox peaks related to the electron transfers of AP was observed and the anodic and cathodic peak currents were much higher than those of bare GCE. The improved electrocatalytic performance of AP may be attributed to the high specific area and excellent conductivity of OMC. After the GCE was modified with ZIF-67, the redox peaks were located at 0.539 and 0.485 V with  $\Delta E_p$  of 54 mV, suggesting that the reversibility of AP at ZIF-67/GCE was greatly improved. While ZIF67–OMC composite was electrodeposited on the GCE surface, the peak–peak potential ( $\Delta E_p$ ) of AP was further decreased to 51 mV and the anodic peak current (10.2  $\mu\text{A}$ ) was nearly five times higher than that at the bare GCE, which further verified the synergic effect between OMC and ZIF-67.

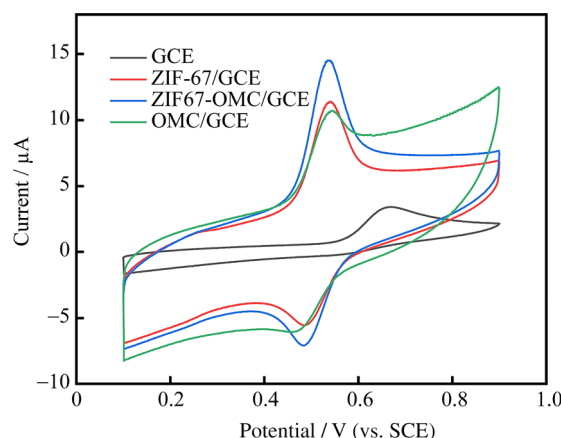


**Fig. 4** CVs of AP ( $0.1 \text{ mmol} \cdot \text{L}^{-1}$ ) at GCE, OMC/GCE, ZIF-67/GCE and ZIF67–OMC/GCE in B–R buffer (pH 4.0) at scan rate of  $100 \text{ mV} \cdot \text{s}^{-1}$

Moreover, the ratio of the anodic peak current to the cathodic peak current ( $I_{pa}:I_{pc}$ ) was  $1.7 > 1$ , indicating that reaction of AP was quasi-reversible reaction process and the ZIF67–OMC composite acted as an effective electrocatalyst for AP.

Figure 5a exhibits the CVs of  $0.1 \text{ mmol} \cdot \text{L}^{-1}$  AP at various scan rates in the range of 40–400  $\text{mV} \cdot \text{s}^{-1}$  to study the electrochemical mechanism of AP at ZIF67–OMC modified electrode. As seen, a pair of well-defined peaks was displayed, and the oxidation and reduction peak currents increased along with the scan rates (Fig. 5a). The linear relationship (Fig. 5b) was attained as:  $I_{pa} = 38.78 \nu^{1/2} - 2.611$  ( $R^2 = 0.992$ ) and  $I_{pc} = -24.85 \nu^{1/2} + 2.654$  ( $R^2 = 0.997$ ), respectively, implying that the redox behavior of AP at the ZIF67–OMC electrode was a typical diffusion-controlled process.

Moreover, the influence of scan rate on peak potential was further investigated for AP (shown in Fig. 5c). The redox peak potentials ( $E_p$ ) were linear to the logarithm of scan rate ( $\lg \nu$ ) ranging from 160 to 400  $\text{mV} \cdot \text{s}^{-1}$  with the equations of  $E_{pa} = 0.0496 \lg \nu + 0.581$  ( $R = 0.984$ ) and  $E_{pc} = -0.0484 \lg \nu + 0.447$  ( $R = 0.981$ ), respectively. And the electron-transfer coefficient ( $\alpha$ ), the electron transfer number ( $n$ ) and the electron transfer rate constant ( $k_s$ ) can be calculated based on the Laviron's equation [42]:

$$E_{pa} = E^0 + \frac{2.3RT}{(1-\alpha)nF} \lg \nu \quad (2)$$

$$E_{pc} = E^0 - \frac{2.3RT}{\alpha nF} \lg \nu \quad (3)$$

$$\lg k_s = \alpha \lg(1-\alpha) + (1-\alpha) \lg \alpha - \lg \frac{RT}{nF\nu} - \alpha(1-\alpha) \frac{nF\Delta E_p}{2.303RT} \quad (4)$$

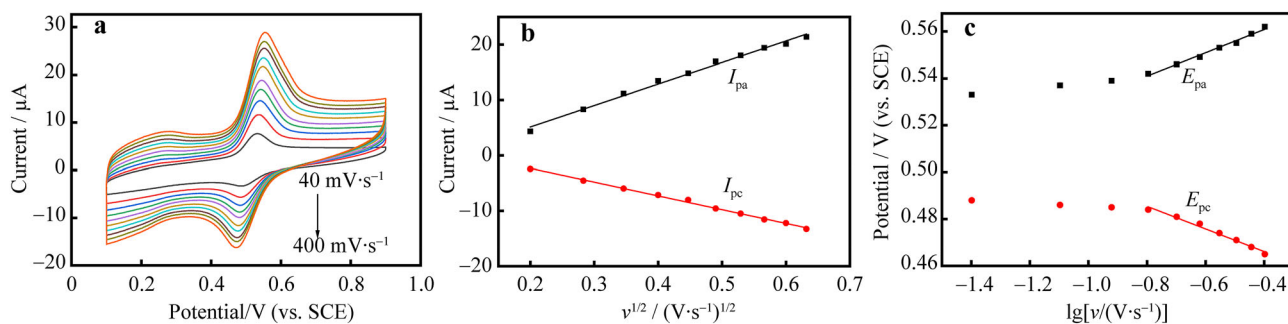


**Fig. 5** a CVs of 0.1 mmol·L<sup>-1</sup> AP in B-R buffer (pH 4.0) at ZIF67-OMC/GCE with different potential scan rates (40–400 mV·s<sup>-1</sup>); b linear relationships of  $I_p$  vs.  $v^{1/2}$  for AP; c plots of  $E_p$  vs.  $\lg v$

where  $v$ ,  $R$ ,  $T$  and  $F$  represent scan rate, molar gas constant, thermodynamic temperature and Faraday's constant, respectively. According to the line's slope of  $E_{pa}$  and  $E_{pc}$ , the values of  $\alpha$ ,  $n$  and  $k_s$  for AP were calculated to be 0.51, 2.22 ( $\approx 2$ ) and 1.42 s<sup>-1</sup>, respectively. The  $k_s$  of the obtained electrode was higher than that of the reported Cu-MOFs/MWCNTAu@Ag/GCE [13]. Thus, the above results revealed that the electron transfer at ZIF67-OMC/GCE was quite fast toward the reaction of AP.

Meanwhile, the electrochemical response of AP (0.1 mmol·L<sup>-1</sup>) at ZIF67-OMC/GCE was further explored in B-R solutions with various pH (2.0–6.0) by CV (Fig. 6a). Clearly, as displayed in Fig. 6b, the anodic peak current of AP obviously increased with an increase in pH from 2.0 to 4.0, reached the peak at pH of 4.0, and then decreased with the increase in pH. The highest peak current of AP was achieved at pH 4.0. N-acetyl-p-benzoquinone-imine could be transformed to p-benzoquinone in protonation reaction and following chemical reaction at low pH [43]. The electrochemical reaction became harder at high pH, owing to the instability of N-acetyl-p-benzoquinone-imine at high pH (4.0–6.0) [44]. Thus, the optimal pH value for AP was selected to be 4.0. Furthermore, the

anodic peak potentials moved to negative values with increased pH in this range, proving that the protons were directly involved in the electrochemical reaction of AP. The linear equation between  $E_{pa}$  and pH was described as  $E_{pa} = 0.7494 - 0.0543 \text{ pH}$  ( $R^2 = 0.999$ ). According to Eq. (5):

$$\frac{dE_p}{dpH} = \frac{2.303mRT}{nF} \quad (5)$$

where  $n$  and  $m$  are the number of the electrons and protons, respectively. The value of  $m/n$  was obtained to be 0.91 ( $\approx 1$ ) from the slope of the  $E_p$ -pH plot, illustrating that the redox reaction of AP at ZIF67-OMC/GCE underwent a two-electron and two-proton process [11, 45]. The reaction mechanism of AP is given in Scheme 1.

### 3.4 Electrochemical determination of AP

As a common electrochemical technique with high sensitivity, differential pulse voltammetry (DPV) was performed to determine AP in this experiment. The DPV curves of AP to various concentrations ( $C$ ) of 0.05 – 100  $\mu\text{mol}\cdot\text{L}^{-1}$  at the obtained ZIF67-OMC/GCE are shown in Fig. 7a. The anodic peak current signal of AP

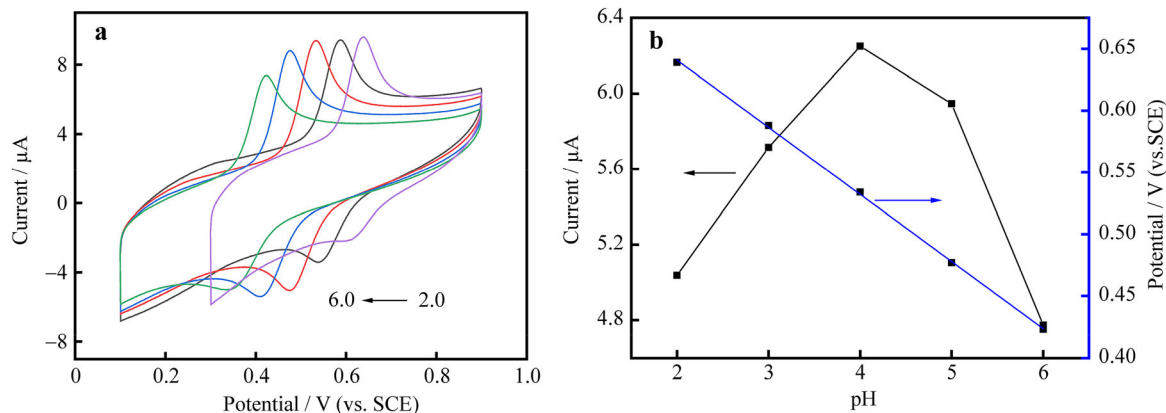


**Fig. 6** a CVs of 0.1 mmol·L<sup>-1</sup> AP in B-R with different pH (2.0–6.0) at ZIF67-OMC/GCE, scan rate of 100 mV·s<sup>-1</sup>; b relationship of pH vs. oxidation peak potentials and peak currents of AP

gradually increased with the concentration ranging from 0.05 to 100  $\mu\text{mol}\cdot\text{L}^{-1}$  (Fig. 7b), and the calibration curve was  $I_{\text{pa}} = 0.1931C + 0.5508$  ( $R^2 = 0.984$ ) with the sensitivity of  $0.1931 \mu\text{A}\cdot(\mu\text{mol}\cdot\text{L}^{-1})^{-1}$ . The limit of detection (LOD) of the ZIF67–OMC sensor was calculated to be  $20 \text{ nmol}\cdot\text{L}^{-1}$  for AP (signal to noise ratio ( $S/N$ ) = 3). Compared with the previously reported sensors for AP (Table 1) [11–14, 16, 44, 45], the sensing ability of ZIF67–OMC sensor was excellent, which holds promising application for the detection of AP.

### 3.5 Interference, reproducibility and stability

In real samples, AP often coexists with dopamine (DA) and ascorbic acid (AA), which are electrochemically active analytes and important interfering substances. The DPV curve of AP ( $50 \mu\text{mol}\cdot\text{L}^{-1}$ ), DA ( $50 \mu\text{mol}\cdot\text{L}^{-1}$ ) and AA ( $300 \mu\text{mol}\cdot\text{L}^{-1}$ ) is displayed in Fig. 8a. The oxidation peak potentials of AP, DA and AA were well separated, which located at 0.460 V (AP), 0.264 V (DA) and 0.184 V (AA). Meanwhile, the current responses of AP at the obtained sensor were higher than those of DA and AA, implying that this sensor had good selectivity for AP detection in the presence of them. In addition,  $i-t$  curve (Fig. 8b) exhibited possible interference with other compounds, including organic compounds (20-fold concentration of glucose, citric acid, tyrosine and twofold concentration of L-cysteine) and inorganic ions (100-fold concentration of NaCl,  $\text{ZnSO}_4$  and  $\text{FeCl}_3$ ). The results manifested that different concentrations of the organic and inorganic analytes had no evident effect (less than 5%) when other substances were added, indicating better selectivity of ZIF67–OMC sensor for AP detection.

The reproducibility of the ZIF67–OMC electrode was also studied in B–R buffer (pH 4.0) containing  $20 \mu\text{mol}\cdot\text{L}^{-1}$  AP for five parallel modified electrodes,

**Table 1** Comparisons of determination performance of AP at obtained ZIF67–OMC/GCE with other reported sensors

Sensor	Linear range/ ( $\mu\text{mol}\cdot\text{L}^{-1}$ )	LOD/ ( $\mu\text{mol}\cdot\text{L}^{-1}$ )	Refs.
AG-NA/GCE <sup>a</sup>	0.05–20	0.031	[11]
FeS/RGO/GCE <sup>b</sup>	5.00–300	0.180	[12]
Cu-MOFs/MWCNT-Au@Ag/GCE	1.00–40, 40–500	0.323	[13]
NiO-CuO/GR/GCE <sup>c</sup>	4.00–100, 100–400	1.330	[14]
PEDOT/GO/GCE <sup>d</sup>	10.00–60	0.570	[16]
GR/GCE <sup>e</sup>	0.10–20	0.032	[44]
Gold nanosheets/GCE	3.00–320	0.230	[45]
ZIF67–OMC/GCE	0.05–100	0.020	This work

<sup>a</sup>Activated graphene-Nafion

<sup>b</sup>FeS-anchored reduced graphene oxide nanosheets

<sup>c</sup>nickel and copper oxides-graphene

<sup>d</sup>poly(3,4-ethylenedioxythiophene)/graphene oxide

<sup>e</sup>graphene

which exhibited good reproducibility with the relative standard deviation (RSD) value of 2.94% for AP. Good interday stability of ZIF67–OMC/GCE was detected by storing it at 4 °C for 15 days. The current signal of the proposed sensor retained  $\sim 92.6\%$  of its initial response, confirming that this modified electrode had acceptable reproducibility and stability.

### 3.6 Determination of real samples

To investigate the potentials of ZIF67–OMC/GCE, it was applied to detect AP in the compound paracetamol tablets and urine samples, which were obtained from local drug-stores and healthy volunteers. The tablets were powdered and dissolved in alcohol with sonication for 30 min, then

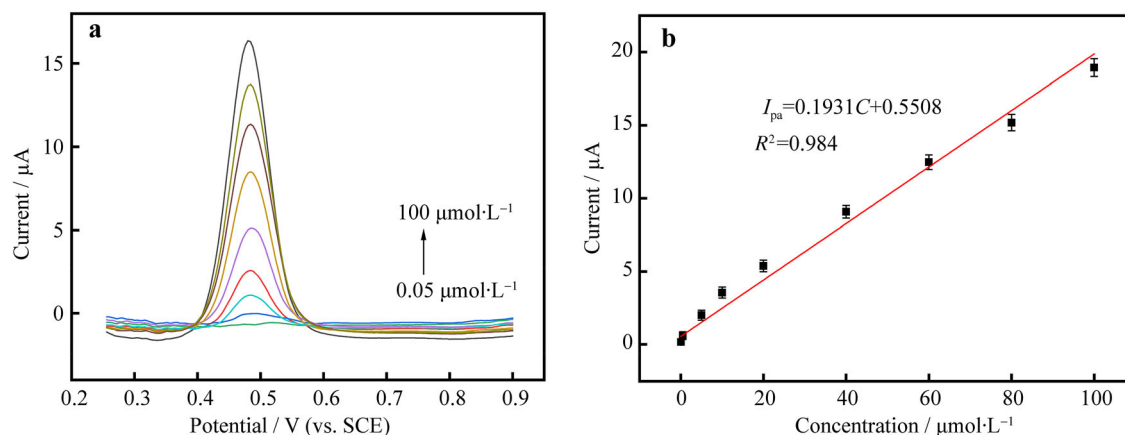


**Fig. 7** a DPV curves at ZIF67–OMC/GCE in 0.05, 0.5, 5.0, 10.0, 20.0, 40.0, 60.0, 80.0 and 100.0  $\mu\text{mol}\cdot\text{L}^{-1}$  AP containing B–R buffer (pH 4.0); b calibration curve between peak current and AP concentration

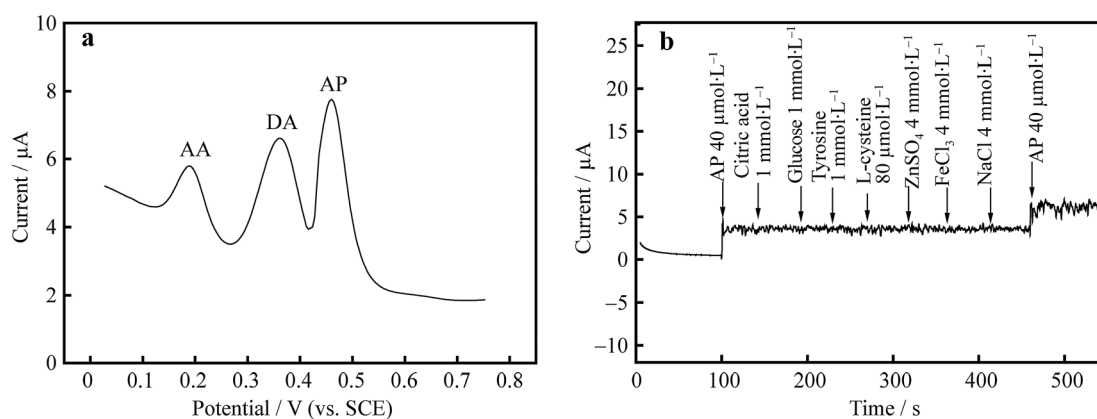


**Fig. 8** a DPV curve of AP ( $50 \mu\text{mol}\cdot\text{L}^{-1}$ ), DA ( $50 \mu\text{mol}\cdot\text{L}^{-1}$ ) and AA ( $300 \mu\text{mol}\cdot\text{L}^{-1}$ ) at ZIF67-OMC/GCE; b  $I-t$  curve of ZIF67-OMC/GCE with subsequent additions of possible interfering at potential of 0.46 V

**Table 2** Determination of AP in compound paracetamol tablets and urine samples ( $n = 3$ )

Sample	Detected/ $(\mu\text{mol}\cdot\text{L}^{-1})$	Spiked/ $(\mu\text{mol}\cdot\text{L}^{-1})$	Found/ $(\mu\text{mol}\cdot\text{L}^{-1})$	RSD <sup>a</sup> /%	Recovery <sup>b</sup> /%
Compound paracetamol tablets	66	5	$71.80 \pm 1.79$	2.5	101.1
		10	$75.22 \pm 2.35$	3.1	98.9
		20	$84.76 \pm 2.97$	3.5	98.6
Urine	—	5	$5.13 \pm 0.21$	4.1	102.6
		10	$9.62 \pm 0.36$	3.7	96.2
		20	$21.08 \pm 0.74$	3.5	105.4

<sup>a</sup>Relative standard deviation for three successive measurements

<sup>b</sup>recovery =  $(C_{\text{found}}/C_{\text{total}}) \times 100\%$

filtered through 0.22- $\mu\text{m}$  pore-diameter membranes. Subsequently, 10  $\mu\text{l}$  of filtrate was diluted to 10 ml with B-R buffer and analyzed by DPV. The urine samples were diluted without any further treatment. In addition, the standard addition method was applied to achieve recovery value. As shown in Table 2, high recoveries were achieved for real samples, which ranged from 96.2% to 105.4%, suggesting that ZIF67-OMC modified electrode was highly suitable for the detection of AP in real samples.

## 4 Conclusion

In conclusion, ZIF67-OMC composite was successfully fabricated by a facile method and modified GCE for sensitive detection of AP. The size of ZIF-67 in situ growth matched well with the macropores of the OMC matrix. The proposed ZIF67-OMC/GCE exhibited excellent electrocatalytic ability toward AP oxidation with high selectivity, good stability and reproducibility. The exceptional electrochemical activity may be attributed to large surface area, increased conductivity and fast electron transport property

of ZIF67-OMC composite. Moreover, the designed ZIF67-OMC/GCE was efficiently used for AP detection in real samples. This facile strategy may offer a new approach to fabricate other MOF composite material sensors.

**Acknowledgements** This work was supported by the National Natural Science Foundation of China (Nos. 21904004 and 11804003), the Domestic Visiting Scholar Program for Outstanding Young Talents of Anhui Province (No. gxgnfx2019019), the Nature Foundation of Anhui Province (No. 1808085MB31), the University Synergy Innovation Program of Anhui Province (Nos. GXXT-2019-043 and GXXT-2019-019) and the Stable Talent Program and the Outstanding Talent Program of Anhui Science and Technology University.

## References

- [1] Graham GG, Scott KF. Mechanism of action of paracetamol. *Am J Ther.* 2005;12(1):46.
- [2] Jefferies S, Saxena M, Young P. Paracetamol in critical illness: a review. *Crit Care Resusc.* 2012;14(1):74.
- [3] Liu GT, Chen HF, Lin GM, Ye PP, Wang XP, Jiao YZ, Guo XY, Wen Y, Yang HF. One-step electrodeposition of graphene loaded nickel oxides nanoparticles for acetaminophen detection. *Biosens Bioelectron.* 2014;56(6):26.

- [4] Glavanović S, Glavanović M, Tomišić V. Simultaneous quantitative determination of paracetamol and tramadol in tablet formulation using UV spectrophotometry and chemometric methods. *Spectrochim Acta A*. 2016;157(6):258.
- [5] Trettin A, Zoerner AA, Böhmer A, Gutzki FM, Stichtenoth DO, Jordan J, Tsikas D. Quantification of acetaminophen (paracetamol) in human plasma and urine by stable isotope-dilution GC–MS and GC–MS/MS as pentafluorobenzyl ether derivative. *J Chromatogr B*. 2011;879(23):2274.
- [6] Nebot C, Gibb SW, Boyd KG. Quantification of human pharmaceuticals in water samples by high performance liquid chromatography–tandem mass spectrometry. *Anal Chim Acta*. 2007;598(1):87.
- [7] Madrakian T, Afkhami A, Mohammadnejad M. Second-order advantage applied to simultaneous spectrofluorimetric determination of paracetamol and mefenamic acid in urine samples. *Anal Chim Acta*. 2009;645(1–2):25.
- [8] Easwaramoorthy D, Yu Y, Huang H. Chemiluminescence detection of paracetamol by a luminol-permanganate based reaction. *Anal Chim Acta*. 2001;439(1):95.
- [9] Radovan C, Cofan C, Cinghita D. Simultaneous determination of acetaminophen and ascorbic acid at an unmodified boron-doped diamond electrode by differential pulse voltammetry in buffered media. *Electroanalysis*. 2008;20(12):1346.
- [10] Ibáñez-Redín G, Wilson D, Gonçalves D, Oliveira ON Jr. Low-cost screen-printed electrodes based on electrochemically reduced graphene oxide-carbon black nanocomposites for dopamine, epinephrine and paracetamol detection. *J Colloid Interf Sci*. 2018;515(42):101.
- [11] Kim D, Lee S, Piao YZ. Electrochemical determination of dopamine and acetaminophen using activated graphene-Nafion modified glassy carbon electrode. *J Electroanal Chem*. 2017;794:221.
- [12] Liu XY, Shangguan EB, Li J, Ning SH, Guo LT, Li QM. A novel electrochemical sensor based on FeS anchored reduced graphene oxide nanosheets for simultaneous determination of dopamine and acetaminophen. *Mater Sci Eng C*. 2017;70:628.
- [13] Chen X, Zhang G, Shi L, Pan S, Liu W, Pan H. Au/ZnO hybrid nanocatalysts impregnated in N-doped graphene for simultaneous determination of ascorbic acid, acetaminophen and dopamine. *Mater Sci Eng C*. 2016;65:80.
- [14] Liu BD, Ouyang XQ, Ding YP, Luo LQ, Xu D, Ning YQ. Electrochemical preparation of nickel and copper oxides-decorated graphene composite for simultaneous determination of dopamine, acetaminophen and tryptophan. *Talanta*. 2016;146:114.
- [15] Alothman ZA, Bukhari N, Wabaidur SM, Haider S. Simultaneous electrochemical determination of dopamine and acetaminophen using multiwall carbon nanotubes modified glassy carbon electrode. *Sens Actuat B*. 2010;146(1):314.
- [16] Si WM, Lei W, Han Z, Zhang YH, Hao QL, Xia MZ. Electrochemical sensing of acetaminophen based on poly(3,4-ethylenedioxythiophene)/graphene oxide composites. *Sens Actuat B*. 2014;193:823.
- [17] Zhao Y, Wang J, Bao Z, Xing H, Zhang Z, Su B, Yang Q, Yang Y, Ren Q. Adsorption separation of acetylene and ethylene in a highly thermostable microporous metal-organic framework. *Sep Purif Technol*. 2018;195:238.
- [18] Liu X, Guan C, Hu Y, Zhang L, Elshahawy AM, Wang J. 2D metal–organic frameworks derived nanocarbon arrays for substrate enhancement in flexible supercapacitors. *Small*. 2018;14(43):1702641.
- [19] Chen XH, Wei Q, Hong JD, Xu R, Zhou TH. Bifunctional metal–organic frameworks toward photocatalytic CO<sub>2</sub> reduction by post-synthetic ligand exchange. *Rare Met*. 2019;38(5):413.
- [20] Zhang S, Zhao YX, Shi R, Waterhouse GIN, Zhang TR. Photocatalytic ammonia synthesis: recent progress and future. *Energy Chem*. 2019;1(2):100013.
- [21] Singh BK, Lee S, Na K. An overview on metal-related catalysts: metal oxides, nanoporous metals and supported metal nanoparticles on metal organic frameworks and zeolites. *Rare Met*. 2019;38(1):1.
- [22] Li DD, Xu HQ, Jiao L, Jiang HL. Metal-organic frameworks for catalysis: state of the art, challenges, and opportunities. *Energy Chem*. 2019;1(1):100005.
- [23] Zhou HJ, Zheng MB, Tang H, Xu BY, Tang Y, Pang H. Amorphous intermediate derivative from ZIF-67 and its outstanding electrocatalytic activity. *Small*. 2020;16(2):1904252.
- [24] Hua W, Sun HH, Xu F, Wang JG. A review and perspective on molybdenum-based electrocatalysts for hydrogen evolution reaction. *Rare Met*. 2020;39(4):335.
- [25] Li XR, Yang XC, Xue HG, Pang H, Xu Q. Metal–organic frameworks as a platform for clean energy applications. *Energy Chem*. 2020;2(2):100027.
- [26] Wang MQ, Ye C, Bao SJ, Zhang Y, Yu YN, Xu MW. Carbon nanotubes implanted manganese-based MOFs for simultaneous detection of biomolecules in body fluids. *Analyst*. 2016;141(4):1279.
- [27] Meng W, Wen YY, Dai L, He ZX, Wang L. A novel electrochemical sensor for glucose detection based on Ag@ZIF-67 nanocomposite. *Sens Actuator B*. 2018;260:852.
- [28] Wang Y, Wang YY, Zhang L, Liu CS, Pang H. Core–shell-type ZIF-8@ZIF-67@POM hybrids as efficient electrocatalysts for the oxygen evolution reaction. *Inorg Chem Front*. 2019;6(9):2514.
- [29] Zhu RM, Ding JW, Xu YX, Yang JP, Xu Q, Pang H.  $\pi$ -conjugated molecule boosts metal–organic frameworks as efficient oxygen evolution reaction catalysts. *Small*. 2018;14(50):1803576.
- [30] Wang HX, Yuan S, Zhou M, Guo LP. A novel electrochemical sensor for detection of baicalein in human serum based on DUT-9/mesoporous carbon composite. *Electroanalysis*. 2020. <https://doi.org/10.1002/elan.201900496>.
- [31] Yao WQ, Guo H, Liu H, Li Q, Xue R, Wu N, Li L, Wang MY, Yang W. Simultaneous electrochemical determination of acetaminophen and dopamine based on metal-organic framework/multiwalled carbon nanotubes-Au@Ag nanocomposites. *J Electrochem Soc*. 2019;166(14):B1258.
- [32] Liang CD, Dai S. Synthesis of mesoporous carbon materials via enhanced hydrogen-bonding interaction. *J Am Chem Soc*. 2006;128(16):5316.
- [33] Li KX, Luo YH, Yu ZX, Deng MH, Li DM, Meng QB. Low temperature fabrication of efficient porous carbon counter electrode for dye-sensitized solar cells. *Electrochem Commun*. 2009;11(7):1346.
- [34] Liang J, Zheng Y, Chen J, Liu J, Hulicova-Jurcakova D, Jaroniec M, Qiao SZ. Facile oxygen reduction on a three-dimensionally ordered macroporous graphitic C<sub>3</sub>N<sub>4</sub>/carbon composite electrocatalyst. *Angew Chem Int Ed*. 2012;124(16):3958.
- [35] Luo LQ, Li F, Zhu LM, Ding YP, Deng DM. Electrochemical sensing platform of natural estrogens based on the poly(l-proline)-ordered mesoporous carbon composite modified glassy carbon electrode. *Sens Actuat B*. 2013;187(1):78.
- [36] Xu B, Shi L, Guo XW, Peng L, Wang ZX, Chen S, Cao GP, Wu F, Yang YS. Nano-CaCO<sub>3</sub> templated mesoporous carbon as anode material for Li-ion batteries. *Electrochim Acta*. 2011;56(18):6464.
- [37] Xu H, Liu F, Cui YJ, Chen BL, Qian GD. A luminescent nanoscale metal-organic framework for sensing of nitroaromatic explosives. *Chem Commun*. 2011;47(11):3153.



- [38] Li XX, Zhu PY, Li Q, Xu YX, Zhao Y, Pang H. Nitrogen-, phosphorus-doped carbon-carbon nanotube CoP dodecahedra by controlling zinc content for high-performance electrocatalytic oxygen evolution. *Rare Met.* 2020;39(6):680.
- [39] Lei Z, Zhang Y, Wang H, Ke Y, Li J, Li F, Xing J. Fabrication of well-ordered macroporous active carbon with a microporous framework. *J Mater Chem.* 2001;11(8):1975.
- [40] Tang J, Jiang SX, Liu Y, Zheng SB, Bai L, Guo JH, Wang JF. Electrochemical determination of dopamine and uric acid using a glassy carbon electrode modified with a composite consisting of a Co(II)-based metalorganic framework (ZIF-67) and graphene oxide. *Microchim Acta.* 2018;185(10):486.
- [41] Zhang YF, Bo XJ, Nsabimana A, Han C, Li M, Guo LP. Electrocatalytically active cobalt-based metal-organic framework with incorporated macroporous carbon composite for electrochemical applications. *J Mater Chem A.* 2015;3(2):732.
- [42] Laviron E. General expression of the linear potential sweep voltammogram in the case of diffusionless electrochemical systems. *J Electroanal Chem Interf Electrochem.* 1979;101(1):19.
- [43] Nematollahi D, Shayani-Jam H, Alimoradi M, Niroomand S. Electrochemical oxidation of acetaminophen in aqueous solutions: kinetic evaluation of hydrolysis, hydroxylation and dimerization processes. *Electrochim Acta.* 2009;54(28):7407.
- [44] Kang X, Wang J, Wu H, Liu J, Aksay IA, Lin Y. A graphene-based electrochemical sensor for sensitive detection of paracetamol. *Talanta.* 2010;81(3):754.
- [45] Zhang QL, Feng JX, Wang AJ, Wei J, Lv ZY, Feng JJ. A glassy carbon electrode modified with porous gold nanosheets for simultaneous determination of dopamine and acetaminophen. *Microchim Acta.* 2015;182(3-4):589.